BIOCHEMISTRY
including biophysical chemistry & molecular biology

Article

pubs.acs.org/biochemistry

Structural and Functional Characterization of the Product of Disease-Related Factor H Gene Conversion

Andrew P. Herbert,[†] David Kavanagh,[†,§] Conny Johansson,[†] Hugh P. Morgan,[‡] Bärbel S. Blaum,[†,∥] Jonathan P. Hannan,[‡,⊥] Paul N. Barlow,[†,‡] and Dušan Uhrín*[,†]

[†]Edinburgh Biomolecular NMR Unit, EastChem School of Chemistry, University of Edinburgh, West Mains Road, Edinburgh EH9 3JJ, U.K.

[‡]Centre for Translational and Chemical Biology, Institute of Structural and Molecular Biology (ISMB), University of Edinburgh, Mayfield Road, Edinburgh EH9 3JR, U.K.

Supporting Information

ABSTRACT: Numerous complement factor H (FH) mutations predispose patients to atypical hemolytic uremic syndrome (aHUS) and other disorders arising from inadequately regulated complement activation. No unifying structural or mechanistic consequences have been ascribed to these mutants beyond impaired self-cell protection. The S1191L and V1197A mutations toward the C-terminus of FH, which occur in patients singly or together, arose from gene conversion between *CFH* encoding FH and *CFHR1* encoding FH-related 1. We show that neither single nor double mutations structurally perturbed recombinant proteins consisting of the FH C-terminal modules, 19 and 20 (FH19-20), although all three FH19-20 mutants were poor, compared to wild-type FH19-20, at promoting hemolysis of C3b-coated erythrocytes through competition with full-length FH. Indeed, our new crystal structure of the S1191L mutant of FH19-20 complexed with an activation-specific complement fragment, C3d, was nearly identical to that of the wild-type FH19-20:C3d complex, consistent with mutants binding to C3b with wild-type-like affinity. The S1191L mutation enhanced thermal stability of module 20, whereas the V1197A mutation dramatically decreased it. Thus, although mutant proteins were folded at 37 °C, they differ in conformational rigidity. Neither single substitutions nor double substitutions increased measurably the extent of FH19-20 self-association, nor did these mutations significantly affect the affinity of FH19-20 for three glycosaminoglycans, despite critical roles of module 20 in recognizing polyanionic self-surface markers. Unexpectedly, FH19-20 mutants containing Leu1191 self-associated on a heparin-coated surface to a higher degree than on surfaces coated with dermatan or chondroitin sulfates. Thus, potentially disease-related functional distinctions between mutants, and between FH and FH-related 1, may manifest in the presence of specific glycosaminoglycans.

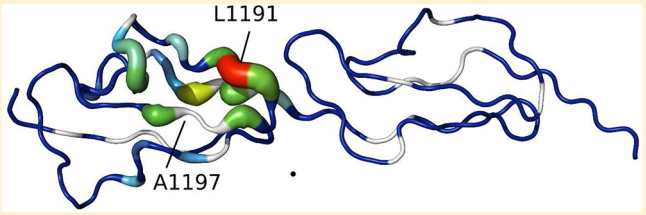

Human factor H (FH) is an abundant (~500 μg/mL) 155 kDa plasma glycoprotein[1] composed from 20 tandem complement control protein modules (CCPs)[2] and encoded by *CFH* on chromosome 1q32. It is the key soluble regulator of the alternative pathway (AP) of complement activation.[3] The AP operates at "tick over" level in the fluid phase and on any surface, self or foreign, resulting in continuous deposition of the potentially self-propagating activation-specific fragment of C3, C3b.[4] Thanks in part to the selective regulatory action of FH, however, C3b is normally amplified exclusively on the foreign surfaces that are the target of complement-mediated effects such as phagocytosis and cytolysis.[5−7]

Factor H recognizes and preferentially binds, via polyanionic surface markers such as sialated species or glycosaminoglycan (GAG) chains, to host surfaces.[8−10] Factor H subsequently assists in the destruction of potentially dangerous host surface-deposited C3 convertases, specific enzymatic complexes that convert inactive C3 to activated C3b. On the other hand, C3 convertases attached to surfaces of invading microbes largely escape this form of regulation. Many human cells carry other homologous AP regulators, which act in a manner similar to that of FH,[11,12] but these are membrane-bound. Consequently, circulating FH is uniquely important for preventing aberrant complement activation via the AP on self-surfaces not enclosed by a cell membrane. Failure, because of mutations and single-nucleotide polymorphisms, of FH to adequately prevent complement amplification on such surfaces is associated with age-related macular degeneration, dense deposit disease, and atypical hemolytic uremic syndrome (aHUS) (reviewed in ref 13). Atypical HUS, linked to numerous mutations in FH,[14,15] is characterized by thrombocytopenia and microangiopathic hemolytic anemia often leading to acute renal failure.[16]

The four N-terminal CCPs of FH (FH1−4) are sufficient to regulate complement in the fluid phase,[17] yet aHUS-associated mutations are predominantly in C-terminal CCPs 19 and 20 (FH19-20),[18] the region responsible for cell surface associa-

Received: November 10, 2011
Revised: February 6, 2012
Published: February 9, 2012

dx.doi.org/10.1021/bi201689j | *Biochemistry* 2012, 51, 1874−1884

tion[19] of FH and for mediating its putative self-association. There are varying reports about the oligomerization state of FH,[20] which may be modulated by its context; e.g., it forms dimers and tetramers in the presence of polyanions,[21] and polyanions enhance function. While CCP 19 (and the CCP 19−CCP 20 junction) binds to the thioester domain (C3d) that C3b uses to tether itself covalently to surfaces,[22,23] CCP 20 binds to nearby GAGs.[24] Thus, these modules are thereby critical for attachment of the protein to targets in the specific context of the self-surface. Modules 1−4 also bind to C3b, while a second GAG-binding site is located on CCP 7,[22,25−27] the site of a single-nucleotide polymorphism (H402Y) strongly linked with age-related macular degeneration.[28−31] The central portion of FH is devoid of binding sites and forms a compact hingelike structure.[32]

Factor H-related proteins (FHR) 1−5 make up a family of proteins, also encoded by genes (*CFHR1*−*CFHR5*) at chromsome 1q32, containing between five and nine CCPs that are very similar or identical to stretches of CCPs in FH (reviewed in ref 33) While the functions of the FHR family are not fully understood, it is noteworthy that genomic deletion of *CFHR1* and *CFHR3* has been associated with an increased risk of aHUS[34] (and a decreased risk of dense deposit disease and age-related macular degeneration). It is particularly interesting that the C-terminal pair of modules from FH and from FHR1 differ by only two amino acids (Ser1191 and Val1197 in FH are replaced in FHR1 with Leu and Ala, respectively) and that these differences correspond to two of the many mutations in FH that have been found in aHUS patients[15] and represent a gene conversion event.[35] Moreover, plasma from a patient heterozygous for the gene encoding S1191L/V1197A FH (i.e., the double mutant of FH) was defective in an assay that measured protection against complement-mediated hemolysis,[35] a hallmark of many aHUS-linked mutants. Five studies have addressed the molecular basis for this deficiency with conflicting conclusions. Jokiranta et al.[36] suggested that these substitutions in FH would disrupt the tertiary structure of CCP 20, while Heinen et al. in 2006[37] and 2009[38] ascribed functional impairment to loss of affinity for C3b; Ferreira et al.[24] and Morgan et al.[23] showed that, within experimental error, S1191L/V1197A FH19-20 (i.e., a recombinant protein fragment corresponding to CCPs 19 and 20 of FH but with Leu at position 1191 and Ala at position 1197) bound C3b as tightly as wild-type FH19-20 did[24] while single mutant S1191L FH19-20 exhibited slightly stronger binding to C3b.

We therefore set out to determine the effects that mutations S1191L and V1197A have on the structure and binding properties of FH19-20. Toward this end, we have studied two C-terminal double-module FH-derived constructs each containing a single amino acid mutation, S1191L FH19-20 and V1197A FH19-20, along with a construct containing a double mutation, S1191L/V1197A FH19-20. We confirmed that while both these mutations, individually or in combination, impaired activity in an FH competition assay and altered thermal stability they had little or no effect on the overall structure of FH19-20 or its mode of interaction with C3d. They did not affect the oligomerization of FH19-20 alone or its affinity for several GAGs. Two of the mutants (S1191L and S1191L/V1197A), however, enhanced the self-association of FH19-20 in the presence of heparin.

EXPERIMENTAL PROCEDURES

Production of Proteins and Hemolysis Protection Assays. Clones of *Pichia pastoris* strain KM71H producing wild-type FH19-20[26] and its mutants[24] were generated as described previously. A detailed protocol for the production of factor H fragments is presented in the Supporting Information. For the purposes of crystallization, recombinant wild-type C3d, corresponding to residues 996−1303 of wild-type human C3d ($C3d_{996-1303}$) and containing an additional C17A (C1010A) point mutation, was produced and purified as previously described.[39,40] Hemolytic assays were conducted as described previously[23,41] and as described in the Supporting Information.

Mass Spectrometry and Nuclear Magnetic Resonance (NMR) Spectroscopy. Mass spectra were acquired on a Voyager-DE STR MALDI-TOF instrument (Applied Biosystems) using standard procedures. Two-dimensional $^{1}H-^{15}N$ HSQC spectra were acquired at 37 °C with 100 μM samples of the FH19-20 proteins in 20 mM deuterated sodium acetate (pH 4.5) containing 10% (v/v) D_2O and 0.02% (w/v) NaN_3. Resonance assignments were determined, where possible, by comparison to the previously assigned wild-type spectrum.[42] Chemical shift differences between the wild-type and mutant proteins were determined using the ANALYSIS module of the common computing protocol for NMR (CCPNMR) software package.[43]

Crystallization and Data Collection. Crystals of C3d in complex with S1191L FH19-20 were grown at 17 °C by the vapor diffusion method from hanging drops using screening conditions similar to those employed for crystallizing the wild-type FH19-20:C3d complex.[23] Drops contained a protein solution in which a complex had been formed with a 1:1 S1191L FH19-20:C3d molar ratio in phosphate-buffered saline (pH 7.4) with an equal volume of well solution. The well solution for the S1191L FH19-20:C3d complex contained 0.1 M Tris-HCl (pH 8.8) and 4% (w/v) polyethylene glycol (8 kDa). Prior to data collection, crystals were cryoprotected with well solution additionally containing 10 and 25% (v/v) glycerol (added stepwise), mounted in loops, and flash-frozen in liquid nitrogen at 77 K.

Intensity data were collected (ϕ scans were 0.5° over 360°) at the Diamond synchrotron radiation facility in Oxfordshire, United Kingdom, on beamline I03. Data were processed in space group *P*1 with MOSFLM[44] and scaled with SCALA.[45] Space group *P*1 was confirmed using POINTLESS, and there was no indication of noncrystallographic symmetry by self-rotation function analysis (Table 1).[45]

Determination of the S1191L FH19-20:C3d Structure. The structure of the S1191L FH19-20:C3d complex was determined by molecular replacement using PHASER[46] with the previously determined structure of the wild-type FH19-20:C3d complex [Protein Data Bank (PDB) entry 3OXU[23,47]] as the search model. There was a clear molecular replacement solution, with three C3d (chains A−C) monomers and three FH19-20 (chains D−F) monomers in the crystallographic asymmetric unit. Crystallographic refinement was performed using PHENIX,[47] first using rigid-body refinement and then a subsequent round of restrained refinement. Areas of disorder were removed at this point from the initial model. Side chains of residues for which no electron density was observed were trimmed back to Cβ stubs using COOT.[48] The model was then subjected to several rounds of restrained refinement, and with the improvement of phases, $F_o - F_c$ electron density

Table 1. Statistics for the S1191L FH19-20:C3d Crystal Structure

Data Collection	
space group	*P*1
cell dimensions	
a, *b*, *c* (Å)	74.75, 82.62, 85.40
α, *β*, *γ* (deg)	112.61, 110.26, 99.84
solvent content (%)	63.62
wavelength (Å)	0.98
resolution	50.47−7.27[a] (2.42−2.30)[b]
no. of reflections	269642
no. of unique reflections	69803
R_{merge} (%)	7.5, 2.9[a] (59.7)[b]
$I/\sigma I$	11.6 (2.2)[b]
R_{meas} (%)	8.7 (69.9)[b]
R_{pim} (%)	4.4 (36.0)[b]
completeness (%)	94.8, 97.4[a] (83.6)[b]
multiplicity	3.9, 3.9[a] (3.7)[b]
Refinement	
no. of C3d monomers per asymmetric unit	3
no. of FH monomers per asymmetric unit	3
no. of working/test reflections	66478/3357
R_{work}/R_{free}	19.05/23.16
average protein *B* factor (Å^2)	56.01
no. of residues	1234
rmsd	
bond lengths (Å)	0.011
bond angles (deg)	0.733
Ramachandran plot (%)	
allowed	96.8
generous	100
disallowed	0

[a]Overall structure, inner shell. [b]Overall structure, outer shell.

corresponding to some of the missing side chains and disordered regions appeared, allowing for manual building and completion. Areas of disorder were carefully modeled into $F_o - F_c$ electron density; the changes in *R* and R_{free} values were used to assess the final model quality, and the progress of refinement was monitored by R_{free}. Water molecules were then added to the model using PHENIX, with several manual additions using COOT, and after several rounds of refinement, the *R* and R_{free} values converged to 19.9 and 24.2, respectively. A further round of translation-libration-screw-restrained refinement using TLSMD[49] yielded final *R* and R_{free} values of 19.05 and 23.16, respectively. The following amino acids, chain A 295-310, chain B 3-9 (where residue 3 in this case is the first residue of the C3d sequence) and 310, chain C 295-310, chain E 1183-1186 and chain F 1175-1178, 1202-1212 and 1229-1231, exhibited no electron density and were not included in the final model. The geometry of the model was assessed using MolProbity,[50] and the coordinates for the 2.35 Å resolution structure have been deposited in the Protein Data Bank as entry 3RJ3. Superimpositions of structures were performed using Pymol (http://www.pymol.org/).

Fluorescence-Based and NMR-Based Assays of Thermal Denaturation. Samples of 20 μM FH19-20 proteins in phosphate-buffered saline (137 mM NaCl, 8.1 mM Na_2HPO_4, 2.7 mM KCl, and 1.5 mM KH_2PO_4) were used for thermal denaturation measurements based on binding to Sypro Orange (Invitrogen).[51] The assays were performed, in triplicate, in 96-well plates in a PTC-100 thermal cycler (Bio-Rad) using a total sample volume of 50 μL/well. The ramp speed was 0.5 °C/s, and dwell times were 30 s. $^1H-^{15}N$ HSQC spectra were recorded on 100 mM samples of ^{15}N-labeled FH19-20 proteins at 5 °C intervals from 25 to 75 °C in 20 mM deuterated sodium acetate (pH 4.5) containing 10% (v/v) D_2O and 0.005% (w/v) NaN_3. Resonances were assigned to groups (by module) and tracked using CCPNMR ANALYSIS.[43]

Gel-Filtration Chromatography. Protein samples (4 μM) were subjected to gel-filtration chromatography on a Superdex 75 HR 10/30 column (GE Healthcare). The chromatography was performed at 4 °C in phosphate-buffered saline supplemented with 5 mM EDTA, at a flow rate of 0.5 mL/min, and protein elution was monitored using OD_{280}. The column was calibrated with the following standards from the low-molecular mass calibration kit (GE Healthcare): vitamin B_{12} (1355 Da), aprotinin (6.5 kDa), ribonuclease A (13.7 kDa), carbonic anhydrase (29 kDa), and ovalbumin (43 kDa).

Isothermal Titration Calorimetry. Dilution isothermal titration calorimetry (ITC)[52] was performed in an Auto-ITC instrument (MicroCal) at 37 °C. A total of 53 μL injections of 1.47 mM wild-type (WT) FH19-20 in phosphate-buffered saline (with 5 mM EDTA) were made into the same buffer in a 1.4 mL calorimetry cell. The injection rate was set to 0.5 μL/min with an interinjection delay of 240 s. The data were fit to a dimer dissociation model using MicroCal Origin.

Biotinylation of GAG and GAG Affinity Chromatography. Bovine lung heparin (Calbiochem), dermatan sulfate (Celsius Laboratories), and chondroitin sulfate C (Fluka) were digested with heparinase I, chondroitinase B, or chondroitinase AC (Grampian Enzymes), respectively, and the hexadecasaccharide fraction was purified by gel filtration on a 26 mm × 1950 mm BioGel P10 column. For biotinylation, 1×10^{-6} mol of hexadecasaccharide was dissolved in 10% H_2O, 20% HOAc, and 70% DMSO in a total volume of 200 μL. Thereafter, 20 μL of freshly prepared 5 M biotinamidohexanoic acid hydrazide (Sigma-Aldrich) in DMSO and 100 μL of 50 mM $NaCNBH_3$ in 50% (v/v) aqueous DMSO were added to the mixture. The reaction mixture was incubated overnight at 65 °C and desalted using a Sephadex G25 superfine column (16 mm × 350 mm) (GE Healthcare).

To confirm that these reaction conditions did not alter the GAG chemical structure, a heparin hexasaccharide was exposed to the same reaction conditions, but in the absence of biotinamidohexanoic acid hydrazide. It was confirmed by strong anion-exchange chromatography and MALDI-TOF mass spectrometry that the reaction conditions did not chemically alter the GAGs. To estimate conjugation efficiency, the absorbance at 232 nm of the desalted GAG was measured before and after loading onto a 1 mL HiTrap streptavidin column (GE Healthcare). The conjugation efficiency varied between ∼70 and 90%.

Glycosaminoglycan affinity chromatography was performed at 4 °C. Protein samples [1 mL of 4 μM in 20 mM HEPES buffer (pH 7.0)] were loaded individually onto the homemade columns, equilibrated with the same buffer, and subsequently eluted with a linear 20 column volume gradient from 0 to 1 M NaCl in 20 mM HEPES buffer (pH 7.0). Protein elution was monitored using OD_{280}.

Surface Plasmon Resonance (SPR)-Based Assays of GAG Binding. Experiments were performed on a T100 SPR instrument (Biacore) at 25 °C in 10 mM HEPES (pH 7.4), 150 mM NaCl, 0.05% (v/v) P20 surfactant, and 3 mM EDTA (HBS-EP$^+$). Streptavidin (New England Biolabs) [588−618

response units (RU)] was coupled to each of the four flow cells of a C1 sensor chip (Biacore) using standard amine coupling. The biotinylated dermatan sulfate (50 RU), chondroitin sulfate C (65 RU), and heparin (44 RU) were immobilized onto streptavidin-coated flow cells 2, 3, and 4, respectively. Injections lasting 4 min were made of each protein over all four of the flow cells at a flow rate of 30 μL/min.

RESULTS

All Three Mutants of FH19-20 Are Functionally Deficient but Structurally Unimpaired. Recombinant (wild-type sequence, i.e., with Ser at position 1191 and Ala at position 1197) FH19-20 inhibits FH-facilitated protection of human and sheep erythrocytes against complement-mediated hemolysis, whereas the single mutant, S1191L FH19-20, and the double mutant, S1191L/V1197A FH19-20, were both previously shown to be much less active in this respect. In the work presented here, the single mutant, V1197A FH19-20, was also tested in this assay, and its activity was found to be impaired but less so than that of either S1191L FH19-20 or S1191L/V1197A FH19-20 (Figure 1).

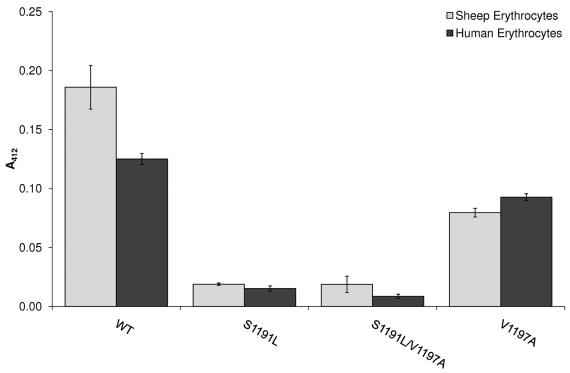

Figure 1. V1197A FH19-20 is functionally deficient. The histogram shows the extent of hemolysis of sheep and human erythrocytes following incubation with normal human sera and 2 μM wild-type or mutant FH19-20 for 20 min at 37 °C.

Two-dimensional ^{1}H−^{15}N HSQC spectra of wild-type and mutant FH19-20 (100 μM) were used to monitor amide chemical shifts (see Figure S1 of the Supporting Information) and line widths (see Figure S2 of the Supporting Information) and hence detect any mutation-induced structural changes. From similarities between spectra (Figure 2A), and from inspecting chemical shift differences (see Figure S1A of the Supporting Information), it was clear that the substitution of Ala1197 with Val (i.e., V1197A) perturbed chemical shifts solely of residues proximal to the substituted residue. No perturbations occurred for resonances arising from CCP 19, or for residues toward the C-terminus of CCP 20 (Figure 2B). Similar results were obtained for S1191L FH19-20, although chemical shift differences (Figure 2C) were greater than they were for V1197A. In the ^{1}H−^{15}N HSQC spectrum of S1191L/V1197A FH19-20, both the number and the size of the perturbations were greater than for either single mutant (see Figure 2D). Nonetheless, the good dispersion and uniform line widths of the ^{1}H−^{15}N HSQC spectrum of the double mutant (Figures S1 and S2 of the Supporting Information) show the protein is compactly folded. Moreover, only seven resonances derived from CCP 19, all located toward its interface with CCP 20, were slightly perturbed; the remaining resonances in CCP

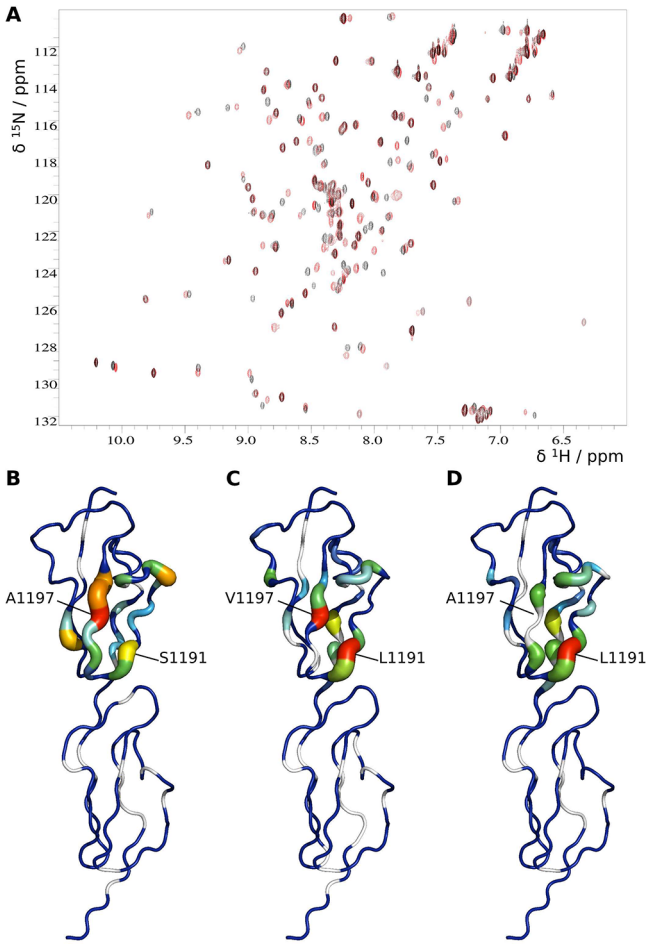

Figure 2. Structural integrity of mutants assessed by ^{1}H−^{15}N HSQC NMR. (A) Overlay of ^{1}H−^{15}N HSQC spectra collected for 100 μM wild-type FH19-20 (black) and V1197A FH19-20 (red). (B−D) For each of the three mutants, combined (^{15}N and ^{1}H) backbone amide chemical shift differences (between wild-type and mutant FH19-20) for individual residues are represented in the context of the three-dimensional structure of FH19-20. The thickness of the cartoon trace varies with the log of the combined chemical shift difference between the mutant and wild type: (B) V1197A FH19-20, (C) S1191L FH19-20, and (D) S1191L/V1197A FH19-20.

19 were unaffected (Figure 2D). Thus, CCP 19 is not structurally compromised by the double mutations in CCP 20, although the possibility of a minor adjustment in intermodular contacts remained. Even in CCP 20, numerous chemical shifts were unperturbed by the double substitution. In summary, these aHUS-linked gene conversion mutations are unlikely to alter significantly the structure of the C-terminus of FH.

The Cocrystal Structure of the S1191L FH19-20:C3d Complex Is Identical to That of the Wild-Type Complex. The site of residue 1191 in CCP 20 is immediately adjacent to the C3b (C3d)-interacting surface that lies mainly on CCP 19 but spans the CCP 19−CCP 20 junction. The side chain of Ser1191 (in the wild-type complex) is buried and does not contribute directly to intermolecular contacts.[23,36,53] Nonetheless, the results of chemical shift perturbation analysis (above) could not exclude the possibility that minor local structural rearrangements, required to accommodate the larger side chain of Leu (in the S1191L mutant), have an impact on C3b recognition as suggested by a previous study using mutated FH18-20. To investigate this possibility, we cocrystallized

dx.doi.org/10.1021/bi201689j | *Biochemistry* 2012, 51, 1874−1884

S1191L FH19-20 with C3d and determined its structure at 2.35 Å resolution.

The structure (Figure 3A) of the S1191L FH19-20:C3d complex is nearly identical to that of the wild-type complex, the

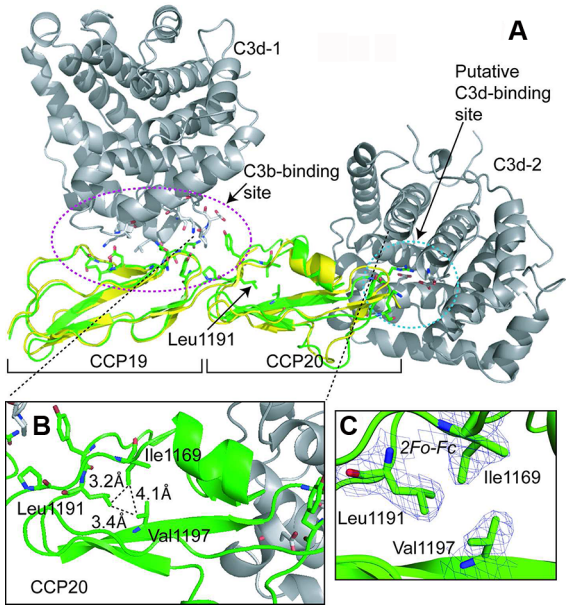

Figure 3. Crystal structure of the FH19-20(S1191L):C3d complex. (A) Cartoon representation of the S1191L FH19-20:C3d complex at 2.35 Å resolution (PDB entry 3RJ3). Colored gray are the two C3d molecules (C3d-1 and C3d-2) that appear in the asymmetric unit; the interaction with C3d-2 may not be physiologically relevant.[23,53] The structure (green) of S1191L FH19-20 is shown superimposed (Cα atoms; rmsd of 0.95 Å) on the structure (yellow) of wild-type FH19-20 (PDB entry 3OXU, chain F). The interfaces between C3d-1 and S1191L FH19-20 and C3D-2 and S1191L FH19-20 (a putative binding site) are colored magenta and cyan, respectively. (B) Stick representation of the increased level of hydrophobic packing that occurs as a result of the substitution of a serine (and a water molecule H-bonded to the serine hydroxyl) with a leucine residue at position 1191. Distances between CD1 of Leu1191 and CD1 of Ile1169, CD1 of Leu1191 and CG2 of Val1197, and CD1 of Ile1169 and CG2 of Val1197 are given (dashed lines). (C) A $2F_o - F_c$ map (blue) highlighting the electron density observed for Leu1191, Ile1169, and Val1197. The resolution of the map is 2.35 Å, and the map is contoured at 1σ.

exception being the substituted residue. The multiple interactions within the asymmetric unit of the cocrystal made between S1191L FH19-20 and C3d are the same as those interactions made by wild-type FH19-20 (Figure.3A). The most extensive of these [with C3d-1 (see Figure 3A)] represents the interaction with C3b.[23] A second heterotypic interaction [with C3d-2 (see Figure 3A)] may be physiologically relevant[53] or might be due to crystal packing. In any case, the crystal structure suggests that the S1191L substitution had no impact on either interaction. The structural details of mutated FH19-20 are consistent with the contribution of Leu1191 and Ala1197 to a tightly packed core within the C-terminal CCP of the paralogous FHR1. The buried leucine side chain directly replaces both the buried serine side chain and a water molecule, observed in the crystal structure of wild-type FH19-20, that is H-bonded to the serine hydroxyl.[36] It lies close to the buried side chain of Val1197 (see Figure 3B,C) [consistent with the amide resonance of this residue having a markedly different chemical shift in the S1191L mutant (see Figure 2C)] such that it might, in the double mutant, help compensate for the replacement of two methyl groups with protons arising from the valine to alanine substitution.

V1197A Destabilizes, but S1191L Stabilizes, CCP 20 of FH19-20. Given the displacement of a buried and H-bonded water molecule from the core of wild-type CCP 20 by the leucine side chain in S1191L FH19-20 and the loss of methyl groups from the CCP 20 hydrophobic core in the V1197A mutant, we investigated what effects these changes have on the thermal stability (parametrized by the midpoint of denaturation, T_m) of FH19-20. Thermal denaturation monitored by fluorescent dye binding (summarized in Table 2) showed that

Table 2. Summary of Inferred T_m Values

FH19-20 variant	whole protein, T_m (°C) by fluororecence quenching	CCP19 alone, T_m (°C) assessed by NMR	CCP20 alone, T_m (°C) assessed by NMR
WT	66	61	62
V1197A	61	56	42
V1197A/S1191L	73	63	71
S1191L	76	64	74

S1191L FH19-20 was more thermally stable than wild-type FH19-20 (ΔT_m = 10 °C) while V1197A FH19-20 was less stable (ΔT_m = −5 °C). The double mutant was more stable than the wild type but only by a ΔT_m of 7 °C. We also investigated by NMR the effects of substitutions on stability of the individual modules within FH19-20 (Figure 4, Table 2, and Figure S3 of the Supporting Information), because precedent[54] suggested that CCPs can melt in a manner that is independent of their neighbors. In this case, T_m was defined as the temperature at which half of the original HSQC cross-peaks, arising from a particular module, remain, i.e., when 50% of the cross-peaks are broadened (due to multiple exchanging conformations) such that they are not detectable. This revealed that CCP 19 and CCP 20 both "melt" at ∼61 °C in wild-type FH19-20. In the case of S1191L FH19-20, both modules were more stable, although the stabilizing effect was modest for CCP 19 (ΔT_m = 3 °C) but striking for CCP 20 (ΔT_m = 12 °C). The double mutant was also more thermally stable than wild-type FH19-20, but the effects were less pronounced, with ΔT_m values of 2 and 9 °C for CCP 19 and CCP 20, respectively. For the V1197A mutant, on the other hand, the destabilizing effect was dramatic for CCP 20 (ΔT_m = −14 °C) and propagated into CCP 19 (ΔT_m = −5 °C). Thus, the C-terminal module of V1197A FH has a T_m of 47 °C; although folded at physiological temperature, it is likely less rigid than the wild type or double mutant, and indeed, some cross-peaks are broadened even at 37 °C.

All Variants Are Monomeric in Solution under Physiological Conditions. It was hypothesized that some aHUS-linked FH mutants malfunction because of inappropriate oligomerization.[36] Wild-type FH19-20 (100 μM) was previously found to be monomeric at 37 °C and pH 4.[42] Only minor changes in spectral properties accompanied titration to pH 7.0 (not shown), suggesting 100 μM FH19-20 does not dimerize appreciably at physiological pH either. Dilution ITC experiments conducted with wild-type FH19-20 further confirmed these observations; the K_D for self-association was calculated to be 6.9 ± 1.0 mM, again indicating that WT FH19-

dx.doi.org/10.1021/bi201689j | Biochemistry 2012, 51, 1874−1884

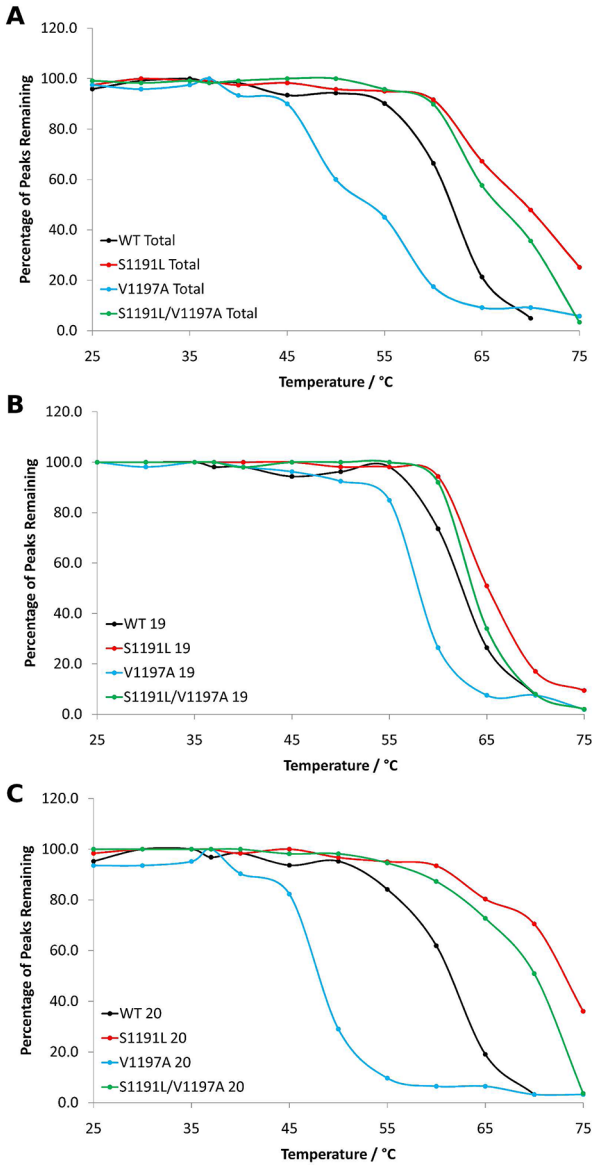

Figure 4. Thermal stability of FH19-20 variants assessed by NMR. (A) Percentages of the maximal numbers of cross-peaks in $^{1}H-^{15}N$ HSQC spectra of (wild-type and mutant) FH19-20 that remained detectable, plotted vs temperature. (B) Like panel A except the plot is based solely on cross-peaks from module 19. (C) Like panel A except the plot is based solely on cross-peaks from module 20. NMR spectra from 55 to 70 °C may be found in Figure S3 of the Supporting Information.

20 is predominantly monomeric at physiological concentrations (data not shown).

We then investigated, using orthogonal methods and a range of conditions, whether S1191L and V1197A FH19-20 differ from WT FH19-20 with respect to self-association properties. The $^{1}H-^{15}N$ HSQC spectra of all three FH19-20 mutants (at 37 °C, low salt, and pH 4.0) resemble those of WT FH19-20 in terms of chemical shift dispersion (Figure S1 of the Supporting Information) and line widths (Figure S2 of the Supporting Information); hence, there is no evidence of self-association under these conditions. Additionally, gel-filtration chromatography was performed at 4 °C and in phosphate-buffered saline on 4 μM samples of all four proteins (in 5 mM EDTA to minimize trace metals that were previously shown to cause uncontrolled oligomerization of full-length fH[55]). It is clear (see Figure 5) from the coelution of all species that there are negligible differences in the oligomerization states of wild-type

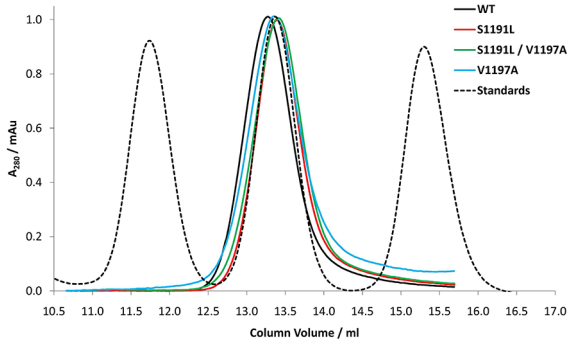

Figure 5. Gel-filtration chromatography of wild-type and mutant FH19-20. Elution profiles, from a calibrated Superdex 75 HR 10/30 column, of 4 μM V1197A FH19-20 (blue), S1191L FH19-20 (red), and S1191L/V1197A FH19-20 (green) are compared with that of wild-type FH19-20 (black). The standards, whose elution profiles are shown here, are ovalbumin (43 kDa) (left-hand peak) and vitamin B_{12} (1355 Da) (right-hand peak).

and mutant FH19-20. Furthermore, the elution volume of each protein from the calibrated column is consistent with that of a monomer.

No Significant Differences in Affinity for Model GAGs between the Wild Type and Mutants. We tested using two approaches whether these aHUS-linked mutations, located in the GAG-binding C-terminus of FH, impaired the affinity of FH19-20 for model GAGs. Affinity chromatography was performed on columns prepared by immobilizing, on streptavidin resin, three types of purified and biotinylated GAG hexadecasacchride fragments. For SPR, "C1" sensor chips were chosen to prevent binding of FH19-20 to the carboxymethlated dextran coating on other chip types. Each flow cell on a single chip was coated with streptavidin, and then the three biotinylated GAGs were individually loaded onto separate flow cells. The SPR responses and GAG affinity chromatograms of wild-type FH19-20 and the three mutants were compared (Figure 6).

Each FH19-20 protein eluted from the dermatan sulfate affinity resin at a similar conductivity (~13 mS cm^{-1}) (see Figure 6A). In SPR studies, all four proteins generated similar responses when passed over dermatan sulfate immobilized on the chip. The profiles of the sensorgrams exhibited fast-on, fast-off kinetics reflecting low affinities typical of protein–GAG interactions that are often in the $10^{-5}-10^{-3}$ M range (Figure 6B). The sizes of the responses are proportional to the number of bound molecules (as well as their molecular mass). Because, judging from the chromatograms, each protein has a similar affinity for dermatan sulfate, the similarity in sizes of responses indicates that all four of the GAG-bound proteins adopt a comparable level of self-association (although we did not establish what this was).

All four proteins interacted more strongly with immobilized chondroitin sulfate C on the resin, eluting at 18 mS cm^{-1} (Figure 6C); this correlates with larger responses obtained by SPR on the chondroitin sulfate-coated chip, although rapid association and dissociation steps are still evident (Figure 6D). Again, therefore, there were no measurable differences between wild-type and mutant proteins either in affinity for this GAG or

dx.doi.org/10.1021/bi201689j | Biochemistry 2012, 51, 1874–1884

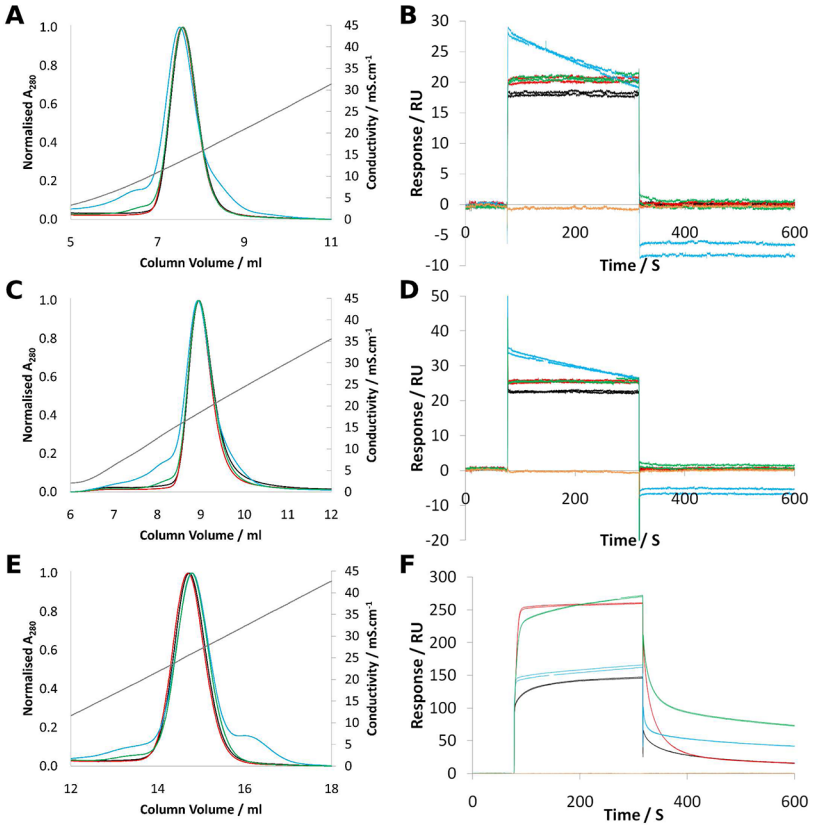

Figure 6. GAG binding measurements for wild-type and mutant FH19-20. (A, C, and E) Overlaid elution profiles, from homemade GAG affinity chromatography columns (for details, see the text), of individually loaded 4 μM samples of wild-type FH19-20 (black), V1197A FH19-20 (blue), S1191L FH19-20 (green), and S1191L/V1197A FH19-20 (red). (A) Elution from the dermatan sulfate affinity column. (C) Elution from the chondroitin sulfate C affinity column. (E) Elution from the heparin affinity column. (B, D, and F) Surface plasmon resonance responses generated by a flow, in duplicate, of wild-type FH19-20 (black), V1197A FH19-20 (blue), S1191L FH19-20 (green), and S1191L/V1197A FH19-20 (red). The buffer trace (orange) over the chip surfaces that had been coupled via streptavidin coupling to (B) dermatan sulfate, (D) chondroitin sulfate C, and (F) heparin.

in the extent of oligomerization of the bound protein molecules.

In the case of heparin, significantly better binding was observed. Each of the FH19-20 proteins eluted from the heparin affinity column at ~27 mS cm^{-1} (Figure 6E), with no difference observed between the binding of the wild type and mutants. The SPR data for heparin binding (Figure 6F) are intriguing because major differences were observed. Both S1191L and S1191L/V1197A FH19-20 produced responses that are ~80% higher than what was observed with respect to wild-type and V1197A FH19-20. The most likely explanation for this observation, in the context of the results of affinity chromatography that clearly indicated equal affinities for all proteins tested, is that binding to the heparin surface is associated with a higher degree of self-association (compared to that of wild-type and V1197A FH19-20) of both S1191L mutants.

DISCUSSION

Recombinant wild-type FH19-20, unlike many of its disease-linked mutants, competes with FH in assays for binding to C3b-coated erythrocytes.[10,24] It inhibits FH-mediated complement regulation and thereby promotes hemolysis. Presumably, the recombinant FH19-20 fragment binds to the same target as the C-terminal region of FH but is subsequently nonprotective because it lacks CCPs 1−4. Our observation that the disease-linked single-site substitution, V1197A, impairs this ability of FH19-20 (see Figure 1) lengthens the list of FH19-20 mutants, which includes S1191L and S1191L/V1197A [reproduced in this study (see Figure 1)], known to be deficient in such an experimental system.[24] The challenge is to find the underlying molecular mechanisms.

Our NMR-based studies (Figure 2) rule out the suggestion[36] that nonconservative substitutions of the buried side chains of Ser1191 and Val1197 in module 20, singly or in combination, significantly disrupt the FH19-20 structure at physiological temperature. We also showed these mutations do not affect oligomerization of the C-terminal portion of FH, in the absence of metal ions or polyanions (Figure 2 and Figure S2 of the Supporting Information).

While the reduction in the thermal stability of V1197A FH19-20 (Figure 4) is striking, it does not provide an obvious explanation for the loss of the ability to compete with FH, given that the S1191L mutation increases thermal stability, yet this mutant is even less functionally active (Figure 1) than V1197A FH19-20. Nonetheless, the decrease in the thermal stability of this critical C-terminal module by 14 °C caused by the Val to Ala substitution is of potentially clinical importance because it is well established that more thermally stable proteins often are less susceptible to proteolysis or chemical modifications. Thus, CCP 20 of V1197A FH has a greater chance of being damaged even while circulating plasma FH levels appear normal in these patients.[15] The fact that the Ser to Leu substitution at position

1191, which inserts methyl groups into the core of CCP 20 and displaces a buried water molecule (see below), restores thermal stability fits nicely with the notion of compensatory mutations and provides a satisfying explanation for the fact that the two residues are both replaced in the equivalent module of FHR1.

Our analysis by X-ray crystallography of S1191L FH19-20 bound to C3d (Figure 3) confirmed that the larger side chain of Leu (compared to that of Ser) was accommodated without conformational adjustment. This is due to the presence of a cavity in wild-type CCP 20 occupied by a water molecule that is H-bonded to the Ser1191 side chain. The orientation between CCPs 19 and 20 remained unaltered (comparing the wild-type FH19-20:C3d complex[23] with the S1191L FH19-20:C3d complex) despite some minor mutation-induced chemical shift perturbations within CCP 19 and propagation of thermally stabilizing or destabilizing effects across the intermodular junction.

Our cocrystal structure also indicates that S1191L FH19-20 recognizes C3d in precisely the same way as wild-type FH19-20. Given the minor and highly localized nature of the chemical shift perturbations induced upon the V1197A substitution, it is safe to assume that the S1191L/V1197A mutant of FH19-20 (and hence also the C-terminal region of CFHR1) will also bind to C3d in this way. This result can be extrapolated to the FH:C3b complex given the lack of overlap between FH1-4 and FH19-20 binding sites on C3b.[23] Thus, these high-resolution structural data are in agreement with previous measurements[23,24] showing that any differences in the affinity of S1191L/V1197A FH19-20 for C3b and C3d, with respect to wild-type FH19-20, would be small. In fact, Morgan et al. found that S1191L-containing mutants bound to C3b and C3d slightly more tightly than wild-type FH19-20.

Thus, our new structural data appear to conflict with reports of deficiencies in C3b and C3d binding by S1191L/V1197A FH.[35,38] The crystal structure, however, does not report on protein dynamics and their putative role during engagement by FH19-20 with C3d. Mutation-induced packing changes in the CCP 20 hydrophobic core, which dramatically modulate its thermal stability, have an impact on the internal conformational mobility of the module, and precedent[56] suggests this could influence C3d binding in subtle ways that are difficult to measure reliably in vitro. In this respect, the S1191L and V1197A substitutions bear comparison with the disease-linked V62I substitution in CCP 1 (part of the N-terminal C3b-binding site of FH), which likewise involves substitution of a buried side chain that does not disturb structure[57] and is not involved directly in contact with C3b.[58] This substitution had a small, difficult-to-detect effect on binding of C3b by FH.[59,60] Indeed, in the case of V62I, functional effects are subtle and probably need to be magnified by other mutations and polymorphisms to substantially raise the risk of disease. In summary, any differences (with respect to the wild type) in the affinity of S1191L/V1197A FH 19-20 for C3b and C3d are slight and are probably inadequate for explaining its poor performance in competing with binding of FH to C3b-coated erythrocytes and almost complete loss of activity in hemolysis protection assays.

Given the lack of structural perturbation or changes to surface charges, it was not unexpected that both single- and double-mutant versions of FH19-20 bound three different model GAGs with affinities indistinguishable from those of wild-type FH19-20 (Figure 6) according to affinity chromatography. This agrees with a previous report[35] that S1191L/V1197A FH did not have diminished heparin binding affinity. Having largely eliminated local structural perturbation, oligomerization in solution, C3d and C3b binding affinity, and affinity for polyanionic cell surface markers, we were left with few other molecular explanations for the striking functional deficiency in S1191L/V1197A FH 19-20. Therefore, our finding that versions of FH19-20 containing the S1191L mutation behaved differently than wild-type FH19-20, and V1197A FH19-20, in the presence of a highly sulfated carbohydrate ligand for CCP 20 is intriguing.

Interestingly, our observations resonate with previous reports by Pangburn et al. of functionally important tetramerization of (wild-type, full-length) FH and FH18-20, in the presence of polyanions, including heparin and dermatan sulfate.[21] There is no obvious structural explanation for why S1191L mutants self-associate on the heparin-coated surface while both wild-type FH19-20 and V1197A FH19-20 apparently do not. Such a clear functional difference between the S1191L and V1197A mutations is nonetheless consistent with the apparently dominant negative nature of S1191L compared to the near-normal functional activity displayed by plasma from a heterozygous V1197A FH patient.[35] It is conceivable that specific GAGs significantly stabilize otherwise very weak self-associations that could not be detected by gel-filtratrion chromatography but have been reported by others[20,36] and appear to be in the millimolar range according to our ITC-based experiments. The consequence is that any differences among the FH19-20 sequence variants in terms of their tendencies to form dimers or tetramers became clearly measurable only in the presence of certain GAGs.

■ CONCLUSIONS

Further work is needed to test whether the S1191L FH19-20 mutants (and FHR1) self-associate on physiologically relevant surfaces and if so whether this prevents them from competing effectively with FH in experimental assays, thus explaining the results depicted in Figure 1. The possibility, apropos of the study of Pangburn et al.,[21] that S1191L mutants of FH in the presence of polyanions form nonfunctional octamers under conditions under which the wild type forms functional tetramers could be investigated. Likewise, the possibility of hetero-oligomer formation involving FH and FH mutants (or indeed FH and FHR1) and any consequences requires further studies. Finally, the implied existence of functional GAG-induced FHR1 homodimers is consistent with the ability of this protein to both bind C3b and to inhibit C5 convertases[38] that contain two (or more) copies of C3b. In summary, functional and structural differences between FH sequence variants may be cryptic and emerge only in specific contexts.

■ ASSOCIATED CONTENT

Supporting Information

Details of protein preparations, hemolysis protection assays, overlays of $^{1}H-^{15}N$ HSQC spectra of the wild type and mutants, plots of line widths for amide proton resonances, combined chemical shift changes for mutants relative to wild-type FH19-20, and thermal denaturation of FH CCPs 19 and 20 monitored by $^{1}H-^{15}N$ HSQC spectra. This material is available free of charge via the Internet at http://pubs.acs.org.

AUTHOR INFORMATION

Corresponding Author

*EastChem School of Chemistry, University of Edinburgh, West Mains Road, Edinburgh EH9 3JJ, U.K. Telephone: 0044-131-650-4742. Fax: 0044-131-650-7155. E-mail: dusan.uhrin@ed.ac.uk.

Present Addresses

[§]Institute of Human Genetics, International Centre for Life, Central Parkway, Newcastle upon Tyne NE1 3BZ, U.K.
[∥]Interfaculty Institute of Biochemistry, University of Tuebingen, Hoppe-Seyler-Str. 4, D-72076 Tuebingen, Germany.
[⊥]Division of Rheumatology, School of Medicine, University of Colorado Denver, 1775 N. Ursula St., Aurora, CO 80045.

Notes

The authors declare no competing financial interest.

ABBREVIATIONS

aHUS, atypical hemolytic uremic syndrome; FH, complement regulatory factor H; FHR1, factor H-related protein 1; GAG, glycosaminoglycan; hr eft, hours elapsed fermentation time; NHS, normal human serum; rmsd, root-mean-square deviation.

REFERENCES

(1) Ripoche, J., Day, A. J., Harris, T. J., and Sim, R. B. (1988) The complete amino acid sequence of human complement factor H. *Biochem. J. 249*, 593−602.

(2) Schmidt, C. Q., Herbert, A. P., Hocking, H. G., Uhrin, D., and Barlow, P. N. (2008) Translational Mini-Review Series on Complement Factor H: Structural and functional correlations for factor H. *Clin. Exp. Immunol. 151*, 14−24.

(3) Pangburn, M. K., Schreiber, R. D., and Muller-Eberhard, H. J. (1977) Human complement C3b inactivator: Isolation, characterization, and demonstration of an absolute requirement for the serum protein β1H for cleavage of C3b and C4b in solution. *J. Exp. Med. 146*, 257−270.

(4) Lachmann, P. J. (2009) The amplification loop of the complement pathways. *Adv. Immunol. 104*, 115−149.

(5) Walport, M. J. (2001) Complement. Second of two parts. *N. Engl. J. Med. 344*, 1140−1144.

(6) Walport, M. J. (2001) Complement. First of two parts. *N. Engl. J. Med. 344*, 1058−1066.

(7) Ricklin, D., Hajishengallis, G., Yang, K., and Lambris, J. D. (2010) Complement: A key system for immune surveillance and homeostasis. *Nat. Immunol. 11*, 785−797.

(8) Meri, S., and Pangburn, M. K. (1990) Discrimination between activators and nonactivators of the alternative pathway of complement: Regulation via a sialic acid/polyanion binding site on factor H. *Proc. Natl. Acad. Sci. U.S.A. 87*, 3982−3986.

(9) Jokiranta, T. S., Zipfel, P. F., Hakulinen, J., Kuhn, S., Pangburn, M. K., Tamerius, J. D., and Meri, S. (1996) Analysis of the recognition mechanism of the alternative pathway of complement by monoclonal anti-factor H antibodies: Evidence for multiple interactions between H and surface bound C3b. *FEBS Lett. 393*, 297−302.

(10) Ferreira, V. P., Herbert, A. P., Hocking, H. G., Barlow, P. N., and Pangburn, M. K. (2006) Critical role of the C-terminal domains of factor H in regulating complement activation at cell surfaces. *J. Immunol. 177*, 6308−6316.

(11) Liszewski, M. K., Farries, T. C., Lublin, D. M., Rooney, I. A., and Atkinson, J. P. (1996) Control of the complement system. *Adv. Immunol. 61*, 201−283.

(12) Kirkitadze, M. D., and Barlow, P. N. (2001) Structure and flexibility of the multiple domain proteins that regulate complement activation. *Immunol. Rev. 180*, 146−161.

(13) de Cordoba, S. R., and de Jorge, E. G. (2008) Translational mini-review series on complement factor H: Genetics and disease associations of human complement factor H. *Clin. Exp. Immunol. 151*, 1−13.

(14) Buddles, M. R., Donne, R. L., Richards, A., Goodship, J., and Goodship, T. H. (2000) Complement factor H gene mutation associated with autosomal recessive atypical hemolytic uremic syndrome. *Am. J. Hum. Genet. 66*, 1721−1722.

(15) Saunders, R. E., Abarrategui-Garrido, C., Fremeaux-Bacchi, V., Goicoechea de Jorge, E., Goodship, T. H., Lopez Trascasa, M., Noris, M., Ponce Castro, I. M., Remuzzi, G., Rodriguez de Cordoba, S., Sanchez-Corral, P., Skerka, C., Zipfel, P. F., and Perkins, S. J. (2007) The interactive Factor H-atypical hemolytic uremic syndrome mutation database and website: Update and integration of membrane cofactor protein and Factor I mutations with structural models. *Hum. Mutat. 28*, 222−234.

(16) Kavanagh, D., and Goodship, T. (2010) Genetics and complement in atypical HUS. *Pediatr. Nephrol. 25*, 2431−2442.

(17) Gordon, D. L., Kaufman, R. M., Blackmore, T. K., Kwong, J., and Lublin, D. M. (1995) Identification of complement regulatory domains in human factor H. *J. Immunol. 155*, 348−356.

(18) Richards, A., Buddles, M. R., Donne, R. L., Kaplan, B. S., Kirk, E., Venning, M. C., Tielemans, C. L., Goodship, J. A., and Goodship, T. H. (2001) Factor H mutations in hemolytic uremic syndrome cluster in exons 18−20, a domain important for host cell recognition. *Am. J. Hum. Genet. 68*, 485−490.

(19) Pangburn, M. K. (2002) Cutting edge: Localization of the host recognition functions of complement factor H at the carboxyl-terminal: Implications for hemolytic uremic syndrome. *J. Immunol. 169*, 4702−4706.

(20) Nan, R., Gor, J., and Perkins, S. J. (2008) Implications of the progressive self-association of wild-type human factor H for complement regulation and disease. *J. Mol. Biol. 375*, 891−900.

(21) Pangburn, M. K., Rawal, N., Cortes, C., Alam, M. N., Ferreira, V. P., and Atkinson, M. A. (2009) Polyanion-induced self-association of complement factor H. *J. Immunol. 182*, 1061−1068.

(22) Schmidt, C. Q., Herbert, A. P., Kavanagh, D., Gandy, C., Fenton, C. J., Blaum, B. S., Lyon, M., Uhrin, D., and Barlow, P. N. (2008) A new map of glycosaminoglycan and C3b binding sites on factor H. *J. Immunol. 181*, 2610−2619.

(23) Morgan, H. P., Schmidt, C. Q., Guariento, M., Blaum, B. S., Gillespie, D., Herbert, A. P., Kavanagh, D., Mertens, H. D., Svergun, D. I., Johansson, C. M., Uhrin, D., Barlow, P. N., and Hannan, J. P. (2011) Structural basis for engagement by complement factor H of C3b on a self surface. *Nat. Struct. Mol. Biol. 18*, 463−470.

(24) Ferreira, V. P., Herbert, A. P., Cortes, C., McKee, K. A., Blaum, B. S., Esswein, S. T., Uhrin, D., Barlow, P. N., Pangburn, M. K., and Kavanagh, D. (2009) The binding of factor H to a complex of physiological polyanions and C3b on cells is impaired in atypical hemolytic uremic syndrome. *J. Immunol. 182*, 7009−7018.

(25) Giannakis, E., Jokiranta, T. S., Male, D. A., Ranganathan, S., Ormsby, R. J., Fischetti, V. A., Mold, C., and Gordon, D. L. (2003) A common site within factor H SCR 7 responsible for binding heparin, C-reactive protein and streptococcal M protein. *Eur. J. Immunol. 33*, 962−969.

(26) Herbert, A. P., Deakin, J. A., Schmidt, C. Q., Blaum, B. S., Egan, C., Ferreira, V. P., Pangburn, M. K., Lyon, M., Uhrin, D., and Barlow, P. N. (2007) Structure shows that a glycosaminoglycan and protein recognition site in factor H is perturbed by age-related macular degeneration-linked single nucleotide polymorphism. *J. Biol. Chem. 282*, 18960−18968.

(27) Prosser, B. E., Johnson, S., Roversi, P., Herbert, A. P., Blaum, B. S., Tyrrell, J., Jowitt, T. A., Clark, S. J., Tarelli, E., Uhrin, D., Barlow, P. N., Sim, R. B., Day, A. J., and Lea, S. M. (2007) Structural basis for complement factor H-linked age-related macular degeneration. *J. Exp. Med. 204*, 2277−2283.

(28) Hageman, G. S., Anderson, D. H., Johnson, L. V., Hancox, L. S., Taiber, A. J., Hardisty, L. I., Hageman, J. L., Stockman, H. A., Borchardt, J. D., Gehrs, K. M., Smith, R. J., Silvestri, G., Russell, S. R., Klaver, C. C., Barbazetto, I., Chang, S., Yannuzzi, L. A., Barile, G. R., Merriam, J. C., Smith, R. T., Olsh, A. K., Bergeron, J., Zernant, J.,

Merriam, J. E., Gold, B., Dean, M., and Allikmets, R. (2005) A common haplotype in the complement regulatory gene factor H (HF1/CFH) predisposes individuals to age-related macular degeneration. *Proc. Natl. Acad. Sci. U.S.A. 102*, 7227−7232.
(29) Edwards, A. O., Ritter, R., Abel, K. J., Manning, A., Panhuysen, C., and Farrer, L. A. (2005) Complement factor H polymorphism and age-related macular degeneration. *Science 308*, 421−424.
(30) Haines, J. L., Hauser, M. A., Schmidt, S., Scott, W. K., Olson, L. M., Gallins, P., Spencer, K. L., Kwan, S. Y., Noureddine, M., Gilbert, J. R., Schnetz-Boutaud, N., Agarwal, A., Postel, E. A., and Pericak-Vance, M. A. (2005) Complement factor H variant increases the risk of age-related macular degeneration. *Science 308*, 419−421.
(31) Klein, R. J., Zeiss, C., Chew, E. Y., Tsai, J. Y., Sackler, R. S., Haynes, C., Henning, A. K., SanGiovanni, J. P., Mane, S. M., Mayne, S. T., Bracken, M. B., Ferris, F. L., Ott, J., Barnstable, C., and Hoh, J. (2005) Complement factor H polymorphism in age-related macular degeneration. *Science 308*, 385−389.
(32) Schmidt, C. Q., Herbert, A. P., Mertens, H. D., Guariento, M., Soares, D. C., Uhrin, D., Rowe, A. J., Svergun, D. I., and Barlow, P. N. (2010) The central portion of factor H (modules 10−15) is compact and contains a structurally deviant CCP module. *J. Mol. Biol. 395*, 105−122.
(33) Jozsi, M., and Zipfel, P. F. (2008) Factor H family proteins and human diseases. *Trends Immunol. 29*, 380−387.
(34) Zipfel, P. F., Edey, M., Heinen, S., Jozsi, M., Richter, H., Misselwitz, J., Hoppe, B., Routledge, D., Strain, L., Hughes, A. E., Goodship, J. A., Licht, C., Goodship, T. H., and Skerka, C. (2007) Deletion of complement factor H-related genes CFHR1 and CFHR3 is associated with atypical hemolytic uremic syndrome. *PLoS Genet. 3*, e41.
(35) Heinen, S., Sanchez-Corral, P., Jackson, M. S., Strain, L., Goodship, J. A., Kemp, E. J., Skerka, C., Jokiranta, T. S., Meyers, K., Wagner, E., Robitaille, P., Esparza-Gordillo, J., Rodriguez de Cordoba, S., Zipfel, P. F., and Goodship, T. H. (2006) De novo gene conversion in the RCA gene cluster (1q32) causes mutations in complement factor H associated with atypical hemolytic uremic syndrome. *Hum. Mutat. 27*, 292−293.
(36) Jokiranta, T. S., Jaakola, V. P., Lehtinen, M. J., Parepalo, M., Meri, S., and Goldman, A. (2006) Structure of complement factor H carboxyl-terminus reveals molecular basis of atypical haemolytic uremic syndrome. *EMBO J. 25*, 1784−1794.
(37) Heinen, S., Sanchez-Corral, P., Jackson, M. S., Strain, L., Goodship, J. A., Kemp, E. J., Skerka, C., Jokiranta, T. S., Meyers, K., Wagner, E., Robitaille, P., Esparza-Gordillo, J., Rodriguez de Cordoba, S., Zipfel, P. F., and Goodship, T. H. (2006) De novo gene conversion in the RCA gene cluster (1q32) causes mutations in complement factor H associated with atypical hemolytic uremic syndrome. *Hum. Mutat. 27*, 292−293.
(38) Heinen, S., Hartmann, A., Lauer, N., Wiehl, U., Dahse, H. M., Schirmer, S., Gropp, K., Enghardt, T., Wallich, R., Halbich, S., Mihlan, M., Schlotzer-Schrehardt, U., Zipfel, P. F., and Skerka, C. (2009) Factor H-related protein 1 (CFHR-1) inhibits complement C5 convertase activity and terminal complex formation. *Blood 114*, 2439−2447.
(39) Shaw, C. D., Storek, M. J., Young, K. A., Kovacs, J. M., Thurman, J. M., Holers, V. M., and Hannan, J. P. (2010) Delineation of the complement receptor type 2-C3d complex by site-directed mutagenesis and molecular docking. *J. Mol. Biol. 404*, 697−710.
(40) Young, K. A., Chen, X. S., Holers, V. M., and Hannan, J. P. (2007) Isolating the Epstein-Barr virus gp350/220 binding site on complement receptor type 2 (CR2/CD21). *J. Biol. Chem. 282*, 36614−36625.
(41) Kavanagh, D., Burgess, R., Spitzer, D., Richards, A., Diaz-Torres, M. L., Goodship, J. A., Hourcade, D. E., Atkinson, J. P., and Goodship, T. H. (2007) The decay accelerating factor mutation I197V found in hemolytic uraemic syndrome does not impair complement regulation. *Mol. Immunol. 44*, 3162−3167.
(42) Herbert, A. P., Uhrin, D., Lyon, M., Pangburn, M. K., and Barlow, P. N. (2006) Disease-associated sequence variations congregate in a polyanion recognition patch on human factor H revealed in three-dimensional structure. *J. Biol. Chem. 281*, 16512−16520.
(43) Vranken, W. F., Boucher, W., Stevens, T. J., Fogh, R. H., Pajon, A., Llinas, M., Ulrich, E. L., Markley, J. L., Ionides, J., and Laue, E. D. (2005) The CCPN data model for NMR spectroscopy: Development of a software pipeline. *Proteins 59*, 687−696.
(44) Leslie, A. G. W. (1992) Recent changes to the MOSFLM package for processing film and image plate data. *Joint CCP4 + ESF-EAMCB Newsletter on Protein Crystallography*, Daresbury Laboratory, Warrington, U.K.
(45) Evans, P. (2006) Scaling and assessment of data quality. *Acta Crystallogr. D62*, 72−82.
(46) McCoy, A. J., Grosse-Kunstleve, R. W., Adams, P. D., Winn, M. D., Storoni, L. C., and Read, R. J. (2007) Phaser crystallographic software. *J. Appl. Crystallogr. 40*, 658−674.
(47) Adams, P. D., Grosse-Kunstleve, R. W., Hung, L. W., Ioerger, T. R., McCoy, A. J., Moriarty, N. W., Read, R. J., Sacchettini, J. C., Sauter, N. K., and Terwilliger, T. C. (2002) PHENIX: Building new software for automated crystallographic structure determination. *Acta Crystallogr. D58*, 1948−1954.
(48) Emsley, P., and Cowtan, K. (2004) Coot: Model-building tools for molecular graphics. *Acta Crystallogr. D60*, 2126−2132.
(49) Painter, J., and Merritt, E. A. (2006) Optimal description of a protein structure in terms of multiple groups undergoing TLS motion. *Acta Crystallogr. D62*, 439−450.
(50) Davis, I. W., Leaver-Fay, A., Chen, V. B., Block, J. N., Kapral, G. J., Wang, X., Murray, L. W., Arendall, W. B. III, Snoeyink, J., Richardson, J. S., and Richardson, D. C. (2007) MolProbity: All-atom contacts and structure validation for proteins and nucleic acids. *Nucleic Acids Res. 35*, W375−W383.
(51) Lo, M. C., Aulabaugh, A., Jin, G., Cowling, R., Bard, J., Malamas, M., and Ellestad, G. (2004) Evaluation of fluorescence-based thermal shift assays for hit identification in drug discovery. *Anal. Biochem. 332*, 153−159.
(52) Lovatt, M., Cooper, A., and Camilleri, P. (1996) Energetics of cyclodextrin-induced dissociation of insulin. *Eur. Biophys. J. 24*, 354−357.
(53) Kajander, T., Lehtinen, M. J., Hyvarinen, S., Bhattacharjee, A., Leung, E., Isenman, D. E., Meri, S., Goldman, A., and Jokiranta, T. S. (2011) Dual interaction of factor H with C3d and glycosaminoglycans in host-nonhost discrimination by complement. *Proc. Natl. Acad. Sci. U.S.A. 108*, 2897−2902.
(54) Kirkitadze, M. D., Krych, M., Uhrin, D., Dryden, D. T., Smith, B. O., Cooper, A., Wang, X., Hauhart, R., Atkinson, J. P., and Barlow, P. N. (1999) Independently melting modules and highly structured intermodular junctions within complement receptor type 1. *Biochemistry 38*, 7019−7031.
(55) Nan, R., Gor, J., Lengyel, I., and Perkins, S. J. (2008) Uncontrolled zinc- and copper-induced oligomerisation of the human complement regulator factor H and its possible implications for function and disease. *J. Mol. Biol. 384*, 1341−1352.
(56) Diehl, C., Engstrom, O., Delaine, T., Hakansson, M., Genheden, S., Modig, K., Leffler, H., Ryde, U., Nilsson, U. J., and Akke, M. (2010) Protein flexibility and conformational entropy in ligand design targeting the carbohydrate recognition domain of galectin-3. *J. Am. Chem. Soc. 132*, 14577−14589.
(57) Hocking, H. G., Herbert, A. P., Kavanagh, D., Soares, D. C., Ferreira, V. P., Pangburn, M. K., Uhrin, D., and Barlow, P. N. (2008) Structure of the N-terminal Region of Complement Factor H and Conformational Implications of Disease-linked Sequence Variations. *J. Biol. Chem. 283*, 9475−9487.
(58) Wu, J., Wu, Y. Q., Ricklin, D., Janssen, B. J., Lambris, J. D., and Gros, P. (2009) Structure of complement fragment C3b-factor H and implications for host protection by complement regulators. *Nat. Immunol. 10*, 728−733.
(59) Pechtl, I. C., Kavanagh, D., McIntosh, N., Harris, C. L., and Barlow, P. N. (2011) Disease-associated N-terminal complement

factor H mutations perturb cofactor and decay-accelerating activities. *J. Biol. Chem. 286*, 11082−11090.
(60) Tortajada, A., Montes, T., Martinez-Barricarte, R., Morgan, B. P., Harris, C. L., and de Cordoba, S. R. (2009) The disease-protective complement factor H allotypic variant Ile62 shows increased binding affinity for C3b and enhanced cofactor activity. *Hum. Mol. Genet. 18*, 3452−3461.
(61) Strobel, S., Abarrategui-Garrido, C., Fariza-Requejo, E., Seeberger, H., Sanchez-Corral, P., and Jozsi, M. (2011) Factor H-related protein 1 neutralizes anti-factor H autoantibodies in. *Kidney Int. 80*, 397−404.

■ NOTE ADDED IN PROOF

During the proof stages we became aware of recent published data from Strobel et. al[61] that showed CFHR1, unlike FH15-20, does not induce lysis in the hemolysis assay. This is consistent with our result for mutant and wild-type FH19-20 in Figure 1.